Metrol. Meas. Syst., Vol. 33 (2026) No. 1, pp. 1–17
DOI: 10.24425/mms.2026.158361

PAN POLSKA AKADEMIA NAUK

METROLOGY AND MEASUREMENT SYSTEMS

Index 330930, ISSN 0860-8229
www.metrology.wat.edu.pl

M&MS

FULLY ONLINE CALIBRATION-COMPENSATION METHOD FOR ROTARY TABLE POSITIONING ERROR

Kairu Shao[1)], Weibin Zhu[1)✉], Yao Huang[2)], Zi Xue[2)], Jin Zhu[3)]

1) China Jiliang University, College of Metrology Measurement and Instrument, Hangzhou, 310018, China
(✉ *zhuweibin@cjlu.edu.cn*)
2) National Institute of Metrology PR China, Beijing, 100029, China
3) Zhejiang Institute of Quality Sciences, Hangzhou, 310018, China

Abstract

The precision rotary table is an angular positioning generator commonly used in the industry. Ensuring its long-term stability of positioning accuracy is a key concern. Researchers have conducted extensive studies on the online calibration and real-time compensation of rotary table positioning errors. However, existing research often involves some offline processing throughout the calibration and compensation stages. Currently, there is very little research on methods in which the entire process of calibrating and compensating rotary table positioning errors is fully online. Therefore, this paper proposes a fully online calibration-compensation method for rotary table positioning errors and develops a rotary table positioning error calibration-compensation system. Based on the Fourier self-calibration principle and the harmonic compensation principle, this method implements online calibration and real-time compensation of positioning errors using a heterogeneous processor. Throughout the entre process, data processing is guaranteed to be online. The experimental results show that the positioning accuracy of the rotary table improved from [−150.0″, 137.9″] to [−1.3″, 1.6″], effectively improving its precision. The proposed method is highly suitable for compact or cost-sensitive precision rotary tables, while also being applicable for spindle condition monitoring.

Keywords: precision rotary table, positioning error, online calibration, real-time compensation.

1. Introduction

Precision rotary tables are commonly-used angular positioning generators, widely applied in CNC machine tools, angular metrology, aerospace, and other fields. These fields generally impose high requirements on the accuracy of positioning of the rotary table. However, the accuracy is often limited by factors such as mechanical structures, mechanical vibration, grating scale errors, and eccentric mounting of gratings. Currently, factors such as load variation and degradation of mechanical structural performance cause the rotary table positioning error to change, necessitating regular calibration. It is a laborious and time-consuming process, therefore achieving online calibration and real-time compensation for rotary table has become a key concern in industry.

Article history: received July 31, 2025; revised October 13, 2025; accepted November 20, 2025; available online February 18, 2026.

Traditional methods for calibrating rotary table positioning errors involve using a polygon or a multi-tooth division table with a mirror combined with an autocollimator, or employing laser interferometers [1]. However, limited by the number of faces in the polygon and the angular resolution of the multi-tooth division table, the number of sample points is constrained, and the calibration procedure is relatively cumbersome, hindering automation. Consequently, metrologists have begun to use ring laser gyroscopes to calibrate rotary tables.[2] Although ring laser gyroscopes offer ultra-high angular resolution and a lower installation requirement, they suffer from issues such as zero drift and temperature drift. Therefore, research on this method remains in its early stages.

All the aforementioned methods require auxiliary reference instruments for calibration. In contrast, the self-calibration method can achieve calibration without reference instruments, attracting significant research attention, and various self-calibration methods have been proposed. Lu *et al.* proposed the *Time-measurement Dynamic Reversal* (TDR) method based on the free-response model of the rotary table. This method calculates the parameters of the free-response model by measuring the pulse width of the encoder signals using a high-frequency clock signal and derives the encoder error based on the circle closure principle and dynamic reversal [3, 4]. Watanabe *et al.* introduced the *Equal-Division-Average* (EDA) method based on the harmonic characteristics of encoders [5]. It employs N read heads uniformly distributed around the grating disc; the sum of their measurement averaged yields the final evaluation result. This method effectively requires non-N-integer harmonic error components. Although computationally simple, achieving a higher accuracy with the EDA method typically requires increasing the number of read heads. Although optimising the arrangement of the read heads can reduce the required number while improving accuracy, this method still requires a relatively large number of read heads, imposing the higher cost requirement [6]. Ishii *et al.* proposed a *Virtual Equal Division Average* (VEDA) method [7]. Leveraging the harmonic characteristics of encoder periodic errors, it achieves the effect of the multi-read-head EDA method using only two read heads. Similarly, based on the periodicity of encoder division errors, Geckeler *et al.* proposed a Fourier method based on transfer functions [8]. This methods requires fewer read heads, while two or more read heads can achieve high-precision calibration. Furthermore, with more than four read heads, it can measure radial error motion [9].

The error curve obtained by calibration typically needs to be compensated for at the feedback end to improve the rotary table positioning accuracy. Wu *et al.* proposed a phase difference filtering method based on the harmonic characteristics of grating *moiré* fringe signals. By filtering out the second, third, and fourth harmonics of these signals, compensation is achieved [10]. Yang *et al.* proposed an error compensation method based on a *Radial Basis Function* (RBF) neural network, utilising its strong local approximation capability for nonlinear mapping and fast learning speed to compensate for displacement [11]. Park *et al.* proposed a linear compensation method based on the mathematical model of encoder signals, improving various parameters through pre-calculation of offset, amplitude, and phase correction [12]. Zhao *et al.* achieved compensation for eccentricity of the encoder by adding several radial code tracks outside of a traditional absolute encoder. Based on the physical model of encoder mounting eccentricity, it indirectly measures the degree of eccentricity [13]. Zhao *et al.* proposed an encoder error compensation method using three calibration read heads and one measurement read head [14]. This method ensures effective identification of the first ten harmonic components of the encoder's angular measurement error, while requiring only an installation tolerance for the read heads. Zhou *et al.* proposed a real-time compensation method based on harmonic analysis [15]. It performs harmonic analysis on the calibrated encoder error curve and uses the *Coordinate Rotation Digital Computer* (CORDIC) algorithm for computation to achieve compensation. Gurauskis *et al.* employed polynomial fitting to compensate for geometric and temperature errors in linear encoders [16]. Comparison with

results from finite element analysis demonstrated the effectiveness of the polynomial fitting method. In the compensation methods mentioned above, data processing generally requires offline handling, and compensation data is typically stored in the form of *lookup tables* (LUTs) in the controller's ROM, imposing certain requirements on the controller's storage capacity [17].

Although traditional cross-calibration methods are reliable, the requirement for auxiliary instruments alters the load conditions of the rotary table, preventing the acquisition of positioning errors during its normal operating state. Among self-calibration methods, the TDR method relies on high rotation speeds of the rotary table, thus remaining primarily in the laboratory stage. While the Fourier method enables self-calibration of positioning errors of the rotary table and has been applied in metrological standards, its data processing still currently depends on offline handling. The EDA method achieves real-time calibration and compensation and has been implemented in numerous devices [18–21]. However, limited by the number of read heads and its inherent principles, EDA exhibits significant suppression of specific low-order harmonics [22], preventing high accuracy in cost-sensitive or compact applications. Researchers have implemented real-time compensation through various approaches such as harmonic fitting and polynomial fitting. Nevertheless, the acquisition and calculation of compensation parameters still rely on cross-calibration methods. To the best of our knowledge [23, 24], research on methods achieving further online processing of both positioning error calibration and compensation of the rotary table remains very scarce.

Therefore, this paper proposes a fully online calibration-compensation method for positioning errors of the rotary table and develops a novel calibration-compensation system. Based on the Fourier self-calibration method, it utilises dual read heads for online calibration. Leveraging the amplitude and phase information from the calibrated rotary table positioning error curve, it employs the CORDIC algorithm for harmonic calculation. This enables long-term online monitoring and compensation of rotary table positioning errors, thus improving the positioning accuracy of cost-sensitive or compact rotary tables.

2. System principle

2.1. Principle of the Fourier method using two read heads

According to ISO 230-1 [1], the rotary table positioning error $\varepsilon(\theta)$ can be defined as:

$$\varepsilon(\theta) = P(\theta) - \theta, \tag{1}$$

where $P(\theta)$ is the actual angular position of the turntable, and θ is the target position. Considering the principle of the circle closure, $\varepsilon(\theta)$ can be treated as a periodic function with a period of 2π. In practical applications, we assume that two read heads are mounted on a common circle surrounding the grating disc, as shown in Fig. 1, with a subtended angle of α between them.

Assume that the signal sampled by read head R_1 is:

$$R_1(\theta) = \theta + \varepsilon(\theta). \tag{2}$$

Therefore, the signal sampled by read head R2 can be expressed by:

$$R_2(\theta) = \theta + \varepsilon(\theta + \alpha). \tag{3}$$

Subtracting these two signals yields the following:

$$\delta_{21}(\theta) = R_2(\theta) - R_1(\theta) = \varepsilon(\theta + \alpha) - \varepsilon(\theta). \tag{4}$$

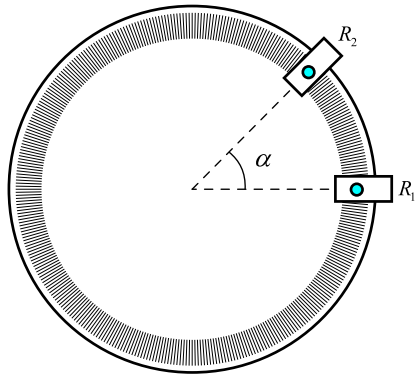

Fig. 1. Diagram of the read head arrangement.

Based on the properties of Fourier series, we obtain:

$$\delta_{21}(\theta) = \sum_{n=-\infty}^{+\infty} \left(e^{jn\alpha} - 1\right) E_n e^{jn\theta}, \tag{5}$$

where, E_n are the Fourier series coefficients of the rotary table positioning error curve $\varepsilon(\theta)$.

Rearranging terms, the transfer function $TF(n)$ can be expressed as:

$$TF(n) = \begin{cases} \frac{1}{\left(e^{jn\alpha}-1\right)}, & e^{jn\alpha} - 1 \neq 0 \\ 0, & \text{otherwise} \end{cases}. \tag{6}$$

Typically, we only analyse the first N harmonic components of the positioning error of the rotary table. Hence, the error curve $\varepsilon(\theta)$ can be represented as:

$$\varepsilon(\theta) = \sum_{n=-N}^{N} E_n e^{jn\theta} = \sum_{n=-N}^{N} D_{21}[n] TF(n) e^{jn\theta}, \tag{7}$$

where $D_{21}[n]$ is obtained by performing the Fourier transform on $\delta_{21}(\theta)$.

In the derivation above, we observe that the transfer function causes harmonic suppression, which affects the calibration accuracy of the Fourier method. The angular interval between read heads is the key variable controlling the behaviour of the transfer function. In our previous research, we conducted a detailed analysis of this angular interval, which yielded the following conclusions [25]: angular separation should avoid circular division points where possible. If unavoidable, the angular separation at the division points should be minimised. Meanwhile, a smaller angular separation improves calibration accuracy but imposes tighter requirements on installation tolerance.

2.2. Principle of harmonic compensation

Using the two-read-head Fourier method, the harmonic order information of the rotary table positioning error can be obtained. This information is used as a compensation value applied to the measured value through series summation. The calculation method is as follows:

$$\theta_{\text{com}}(\theta) = R(\theta) - \varepsilon(\theta) \approx R(\theta) - \varepsilon\left(R(\theta)\right) \tag{8}$$

where $R(\theta)$ is the measured value from the reference read head, and θ_{com} is the compensated measurement value of the rotary table. The rotary table positioning error $\varepsilon(\theta)$, obtained with the Fourier method, provides harmonic information in complex form. Using polar coordinates, it can be converted into a sum of cosine functions:

$$\varepsilon(\theta) = \sum_{n=-N}^{N} E_n e^{jn\theta} = a_0 + 2\sum_{n=1}^{N} A_n \cos(n\theta + \Phi_n), \tag{9}$$

where $A_n = |E_k|$, $\Phi_n = \angle E_n = \tan^{-1}\dfrac{\text{Im}[E_n]}{\text{Re}[E_n]}$.

Common numerical methods for trigonometric functions include polynomial expansion and coordinate rotation. To meet real-time error compensation requirements, all calculations must be implemented in the hardware circuitry. Therefore, this paper employs the CORDIC for trigonometric calculations. The CORDIC method iteratively approximates the target angle through vector rotation [26]. Its iterative calculation formulas are as follows:

$$\begin{cases} x_{i+1} = x_i - y_i \cdot d_i \cdot 2^{-i} \\ y_{i+1} = y_i - x_i \cdot d_i \cdot 2^{-i} \\ z_{i+1} = z_i - d_i \tan^{-1}\left(2^{-i}\right) \end{cases}, \tag{10}$$

where $d_i = -1$, if $z_i < 0$; $+1$, otherwise.

The initial conditions are as follows:

$$\begin{cases} x_0 = \dfrac{1}{A_n} \\ y_0 = 0 \\ z_0 = \varphi \end{cases}, \tag{11}$$

where $A_n = \prod_n \sqrt{1 + 2^{-2i}}$, then after n iterations, the results are:

$$x_n \approx \cos\varphi, \quad y_n \approx \sin\varphi. \tag{12}$$

In practical circuit implementations, the selection of the iteration count and the register bit-width affects the calculation accuracy of the CORDIC algorithm. Related discussions are provided in the appendices.

3. Design of the positioning error calibration-compensation system

To ensure real-time performance of the rotary table positioning error calibration-compensation system, we selected the Xilinx XC7Z020CLG400-2 as the hardware platform [27]. It features 85k logic cells, 4.9 Mb of block RAM, and a dual-core ARM Cortex-A9 MPCore processor. A custom-designed FPGA circuit board is shown in Fig. 2. Based on the self-calibration principle of the two-read-head Fourier method and the harmonic compensation principle, a rotary table positioning error calibration-compensation system was designed using the custom FPGA board. The system block diagram is shown in Fig. 3.

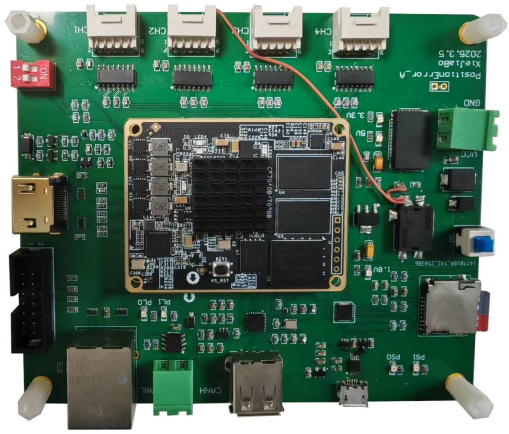

Fig. 2. Photograph of the custom-designed FPGA circuit board.

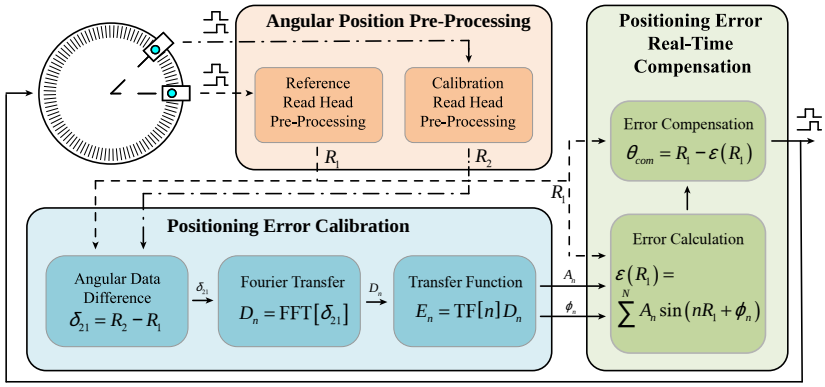

Fig. 3. Diagram of the rotary table positioning error calibration-compensation system.

As seen in Fig. 3, the system can be divided into three subsystems: the rotary table angular position pre-processing system, the rotary table positioning error self-calibration system, and the rotary table positioning error real-time compensation system. The rotary table is equipped with two read heads mounted at fixed angular intervals. One read head serves as the reference; its output measurement signal is used as the control feedback signal. After being processed with the error compensation system, this signal is connected to the rotary table servo feedback system. The other read head serves as the calibration read head and connects to the error calibration system. Its output measurement signal is used solely for calibration and does not directly participate in the motion control of the rotary table. As established in Section 2.1, the Fourier method requires prior knowledge of the angular interval between the two read heads. In our previous work, we identified this angular interval α – the sole variable in the transfer function as the critical parameter determining the calibration accuracy of the Fourier method. Based on conclusions from our previous research [25], we set the angular interval between the two read heads to 33°.

3.1. Design of the angular position pre-processing system

To ensure real-time acquisition of angular data, the rotary table employs an incremental encoder. Through electronic interpolation, the read head outputs two quadrature square waves, as shown in Fig. 4.

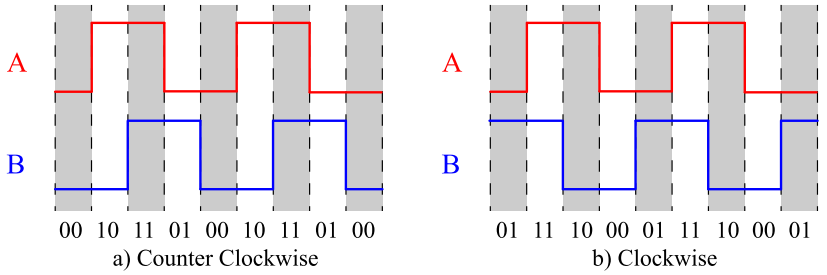

Fig. 4. Diagram of the square wave signal output from read heads.

Figure 4a shows the state of the two square wave signals during the counter-clockwise rotation of the table. Here, signal A leads signal B by 90°, and the level change sequence is 00, 10, 11, 01. Figure 4b shows the state during the clockwise rotation. Here, signal A lags signal B by 90°, and the level change sequence is 00, 01, 11, 10. Based on this behaviour, the relative angular motion of the rotary table is recorded by counting the edges of the two square waves. The direction of motion of the rotary table is determined by judging the phase relationship between the two signals. The reference zero position of the rotary table is established by an index signal. Based on the logical relationship between these signals, the circuit structure for the rotary table signal pre-processing system was designed, as shown in Fig. 5.

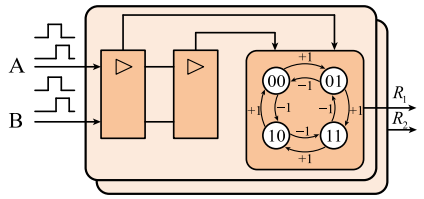

Fig. 5. Circuit structure of the angular position pre-processing system.

As shown in Fig. 5, this circuit features two identical structures. They process the output signals from the two read heads in parallel and output the results to subsequent systems.

3.2. Design of the positioning error self-calibration system

The self-calibration system for rotary table positioning error internally generates a 1 kHz sampling clock signal. At the rising edge of each sampling clock signal, it latches the angular position values from the two read heads output by the pre-processing system and writes them into BRAM. As is known from Section 2.1, the self-calibration process using the Fourier method is complex, therefore implementing this calculation directly into circuitry would result in high complexity and significant difficulty in development. However, leveraging the heterogeneous architecture of the ZYNQ platform, the calibration algorithm is executed on the CPU, ensuring circuit simplicity. After the rotary table completes one full rotation, the CPU reads the data

measured by both read heads from the BRAM, performs calibration using the Fourier method, and subsequently updates the compensation parameters in the positioning error real-time compensation system via BRAM. This update transmits the calculated amplitude and phase information for each harmonic order. The circuit structure of this system is shown in Fig. 6.

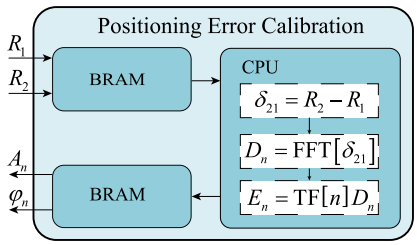

Fig. 6. Circuit structure of positioning error self-calibration system.

During the rotation of the table, the circuit performs equidistant sampling, collecting 12000 data points per full rotation, with a sampling interval of approximately 108″. Since the data length is divisible by the full circle, spectral leakage is effectively suppressed, thereby ensuring data reliability. Prior to calibration calculations, the data stored in BRAM must still be verified, primarily by checking whether the difference between adjacent sampling points is around 108″.

Generally, rotary table positioning error changes are low-frequency and gradual, without sudden shifts. Therefore, we consider our calibration system to be real-time and online. Additionally, functionalities such as human-computer interaction can be implemented on the CPU, enhancing the system's practicality.

3.3. Design of the positioning error real-time compensation system

While ensuring real-time calibration of positioning errors of the rotary table, guaranteeing its positioning accuracy critically depends on the real-time compensation of these errors. This aspect demands an even better real-time performance, which requires the compensation system to exhibit low latency and high processing speed. Therefore, we have designed the real-time error compensation system for the rotary table positioning shown in Fig. 7.

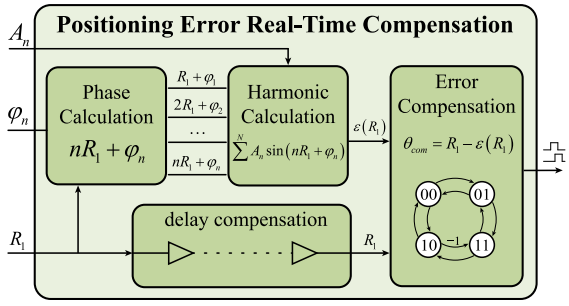

Fig. 7. Circuit structure of the real-time positioning error compensation system.

As seen in Fig. 7, the real-time compensation system consists primarily of four computational units: the phase calculation unit, the harmonic calculation unit, the delay compensation unit and the error compensation unit. The rotary table angular position pre-processing system inputs the value from the reference read head into the phase calculation unit. The phase calculation unit reads

the updated phase information for each harmonic order from the self-calibration system. Using multipliers, LUTs, and adders, it calculates the angle values for each harmonic order in parallel. The structure of this unit is shown in Fig. 8.

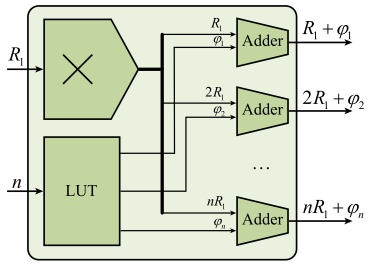

Fig. 8. Structure of the phase calculation unit.

The function of the harmonic calculation unit is to compute the values of each harmonic order based on the angle values provided by the phase calculation unit. Following the CORDIC trigonometric calculation principle mentioned in Section 2.2, a pipelined architecture is designed as shown in Fig. 9. Using simple shifters, adders, and LUTs, it obtains the cosine values for each harmonic order after 16 iterations. The selection of the iteration count and the register bit-width affects the calculation accuracy of the CORDIC algorithm. Related discussions are provided in the appendices.

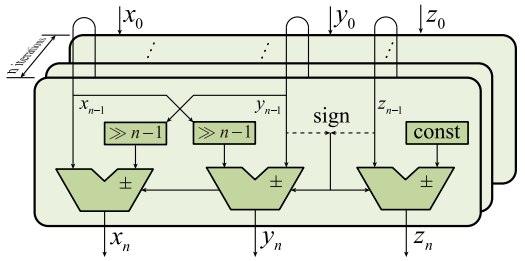

Fig. 9. Pipeline structure of the CORDIC algorithm.

Since both the phase calculation unit and the harmonic calculation unit employ pipelined computation, a delay is introduced in the processing. This means that at any given moment, the harmonic value output from the harmonic calculation unit does not correspond to the angle value input at that same moment. Therefore, the delay compensation unit delays the input angle value. The duration of this delay matches the total computation time of the phase and harmonic calculation units. At this point (after the delay), the angle value output from the delay compensation unit and the harmonic value output from the harmonic calculation unit have a one-to-one correspondence. The delay compensation unit consists solely of multiple buffers.

The error compensation unit calculates the compensation value using angle information from the delay compensation unit and harmonic values from the harmonic calculation unit, according to (8). Finally, based on the relationship between the angle value and the signals shown in Fig. 5, it outputs the rotary table signal that incorporates the compensation value.

Table 1 summarises the delay amount for each unit. As indicated in Table 1, the real-time compensation system introduces a final delay of 29 clock cycles. Considering that the circuit clock frequency is 100 MHz, the system delay is 290 ns. This is far below the update frequency of the read head signals. Therefore, it can be considered that the real-time compensation system exhibits high real-time performance.

Table 1. Delay lengths for each unit in the real-time compensation system.

Unit	Phase calculation unit	Harmonic calculation unit	Error compensation unit
Delay clock period	5	20	4
Delay time	50 ns	200 ns	40 ns

4. Experiment and discussion

This section presents the developed rotary table positioning error calibration-compensation system, as shown in Fig. 10. In Fig. 10a, the rotary table utilises a MicroE PurePrecision grating disc and two M3000 read heads to provide angular position feedback signals. The grating disc has a diameter of 107.95 mm and features 16,384 grating lines over its entire circumference, which corresponds to an approximate grating pitch of 20 µm. The two read heads are mounted around the grating disc at 33° interval with ±50″ installation tolerance (considering the result in our previous work [25]). The angular installation interval and tolerances of the read heads are precisely determined and controlled through a purpose-built mechanical structure and tight machining tolerances. Each read head incorporates a 1024× electronic interpolator, resulting in an overall rotary table angular resolution of 0.772″. The rotary table motion controller (shown in Fig. 10b) integrates components that include a switching power supply, a motor driver, and a display. It enables functionalities such as rotary table position control and human-machine interaction. The switching power supply provides DC power to the entire system. The motor driver uses an ACS SPiiPlus motion controller for motion control of the rotary table. Positioned adjacent to the rotary table motion controller in Fig. 10b, the calibration-compensation system processes signals from the read heads and feeds back the processed signals to the rotary table motion controller. It utilises a custom-designed circuit board (shown in Fig. 2) incorporating the circuits described in Section 3 for real-time compensation and feedback of the angular position signals for the rotary table.

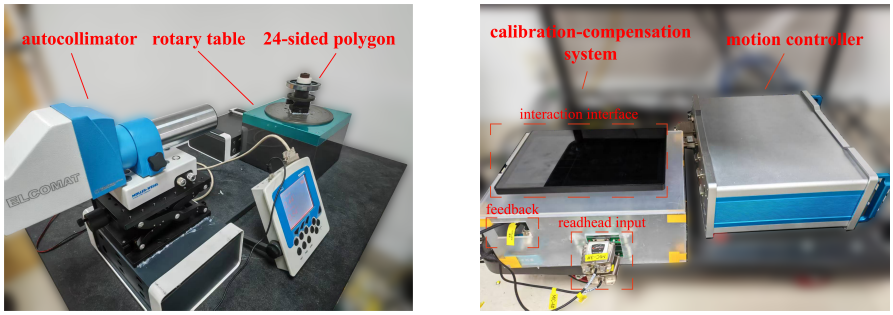

(a) (b)

Fig. 10. Rotary table positioning error calibration-compensation system and experimental platform: a) the rotary table with experimental facilities, b) the calibration-compensation system and the motion controller.

We used a 24-sided polygon and an autocollimator, which is an ELCOMAT 3000, to measure the positioning accuracy of the rotary table before and after activating the positioning error calibration compensation system, which is shown in Fig. 10a. Experiments were conducted in a temperature-controlled environment maintained at 20°C ± 2°C. The accuracy of the measuring equipment is shown in Table 2.

Metrol. Meas. Syst., Vol. 33 (2026), No. 1, pp. 1–17
DOI: 10.24425/mms.2026.158361

Table 2. Specifications of the measuring equipment in the experiment.

Device	Model	Range	Uncertainty ($k = 2$)
Autocollimator	ELCOMAT3000	±1000″	±0.1″
Polygon	24-sided polygon	0° ~ 360°	±0.2″

First, we measured the positioning accuracy of the rotary table without compensation by the calibration-compensation system. Subsequently, we activated the system's online calibration-compensation function and measured the positioning accuracy again. Each measurement comprised sampling points equal to the number of polygon faces. Both scenarios underwent ten measurement cycles to evaluate the positioning repeatability of the rotary table system. The final results are shown in Fig. 11a, where the red curve represents the positioning error of the rotary table without the proposed compensation system, and the blue curve shows the error after compensation.

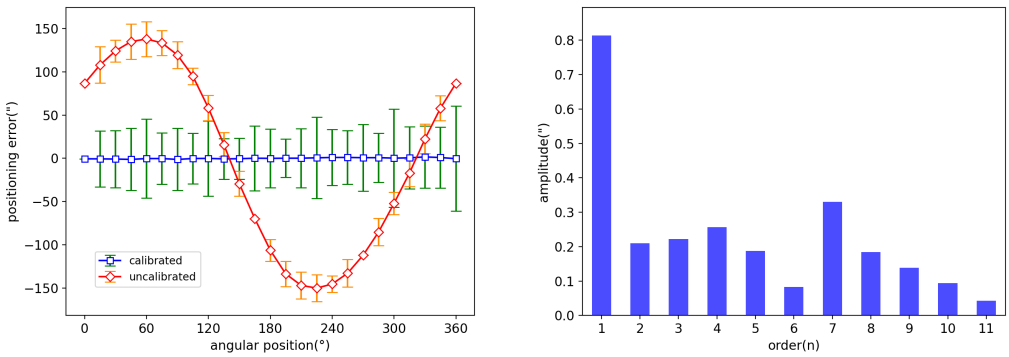

(a) (b)

Fig. 11. Measurement results of the autocollimator and polygon measurement (a) (Standard Deviation 300× Scale Factor) and (b) harmonic analysis.

Repeatability at 24 measurement points is expressed by the standard deviation of individual measurements. The standard deviation estimate is given by Bessel's formula:

$$\sigma = \sqrt{\frac{\sum (x_i - \bar{x})^2}{n-1}}, \tag{13}$$

where x_i denotes the measured values, $\bar{x}$ their mean, and n the number of measurements ($n = 10$ in this experiment). The standard deviation of ten repeated measurements at each angular position was evaluated using this formula and is displayed with 300× visual scaling in Fig. 11a. Figure 11a indicates that the maximum standard deviation does not exceed 0.2″, which resides within one order of magnitude of minimum resolution of the rotary table. Thus, the angular position errors obtained from ten measurements exhibit consistently high reliability.

Figure 11 shows that after compensation with the proposed system, the positioning accuracy of the rotary table improved from $[-\mathbf{150.0}'', \mathbf{137.9}'']$ to $[-\mathbf{1.3}'', \mathbf{1.6}'']$. The harmonic analysis of residual positioning error (Fig. 11b) shows no distinct harmonic characteristics overall, although the first-order harmonic remains relatively high compared to the others, likely due to installation

eccentricity of the polygon. In addition to this, the remaining harmonics exhibit no clear pattern, indicating that random errors serve as the primary residual source. This confirms the effective compensation of most positioning error components. The system successfully enables online calibration and compensation of rotary table positioning errors, significantly improving accuracy. Measurement uncertainty may also contribute to residual errors; its analysis follows.

In the experimental platform, uncertainty sources include polyhedron measurement errors, autocollimator measurement errors, measurement repeatability errors, polyhedron mounting eccentricity, and polyhedron tower difference. These uncertainty components are summarised in Table 3. The calculated expanded uncertainty $U$is $0.46''$, one order of magnitude smaller than the residual positioning error post-compensation. This verifies the reliability of the experimental results and conclusions.

Table 3. Summary of measurement uncertainty.

No.	Sources of uncertainty	Symbol	Type of assessment	Standard uncertainty ($''$)
1	Polyhedron measurement error	u_1	B	0.1
2	Autocollimator measurement error	u_2	B	0.05
3	Measurement repeatability error	u_3	A	0.2
4	Polyhedron mounting eccentricity	u_4	A	0.0005
5	Polyhedron tower difference	u_5	A	0.0001
Combined standard uncertainty $u = 0.23''$ Expanded measurement uncertainty $U = 0.46''$				

The standard measurement uncertainty caused by polyhedron measurement errors and autocollimator measurement errors is provided by the metrology institution, with values of $0.1''$ and $0.05''$ respectively. The standard measurement uncertainty from measurement repeatability equals the mean variance of angular position errors calculated using Bessel's formula, resulting in $0.2''$. The uncertainty induced by the mounting eccentricity of the polygonal mirror depends on the flatness of the surface and the size of the reflector, calculated as [28]:

$$u_4 = \frac{8sh}{H^2}\rho, \tag{14}$$

where s represents the mounting eccentricity distance, h denotes the surface flatness error, H is the reflector width, and ρ is the radian-to-arcsecond conversion constant 206265. In the experimental setup, we controlled $s \leq 1$ µm. With $h = 0.03$ µm and $H = 10$mm, the resulting standard uncertainty $u_4 = 0.0005''$.

Tower difference refers to the installation tilt of the polygonal mirror. Its induced uncertainty is [28]:

$$u_5 = \sin\alpha \frac{\sin^2\tau}{\cos\tau}\rho, \tag{15}$$

where α denotes the working angle of 15° for the 24-sided polygon and τ indicates the maximum tilt angle between the mirror and the axis, controlled within $8''$. Thus, $u_5 = 0.0001''$.

Since these uncertainty components are uncorrelated with zero correlation coefficients, the combined standard uncertainty is:

$$u = \sqrt{u_1^2 + u_2^2 + u_3^2 + u_4^2 + u_5^2} \approx 0.23''. \tag{16}$$

Assuming a normal distribution with $k_{95} = 2$, the expanded uncertainty is:

$$U = u \times k_{95} = 0.46''. \tag{17}$$

5. Conclusions

To ensure rotary table positioning accuracy, this paper proposes a fully online calibration-compensation method for positioning errors. Based on the principles of Fourier-method self-calibration and harmonic error compensation and leveraging the low-latency, high-speed characteristics of hardware circuitry, a rotary table positioning error calibration-compensation system was developed. This system achieves online calibration and real-time compensation of positioning errors of the rotary table. Experimental results show that the positioning error of the rotary table decreased from $[\mathbf{-150.0''}, \mathbf{137.9''}]$ to $[\mathbf{-1.3''}, \mathbf{1.6''}]$ after compensation, demonstrating that the proposed system effectively reduces the positioning error and improves the accuracy of the rotary table.

The proposed method imposes specific requirements on the read head mounting positions; consequently, its effectiveness in improving the accuracy of existing rotary tables may not be significant. However, the developed system enables long-term online monitoring, calibration, and compensation of rotary table positioning accuracy, thereby improving the precision of compact or cost-sensitive rotary tables. Moreover, this method can provide reliable data support for spindle condition monitoring and fault inspection.

6. Acknowledgements

This work was financially supported by the project of the National Key R&D Programme of China (2023YFF0615703), the National Natural Science Foundation of China (52175526), and the Zhejiang Provincial Natural Science Foundation (TGC24E050001).

A. Appendices

The CORDIC algorithm is fundamentally a numerical iterative approximation method. In practical circuits, its calculation accuracy is affected by iteration count n and data bit-width b, leading to computational errors. Limited iteration counts n introduce an approximation error δ, while finite data bit-width b causes a rounding error ϵ.

Based on the CORDIC computational principle, it can be inferred that the approximation error does not exceed the rotation angle in the final iteration. Thus, the maximum approximation error $\delta_{\max}$ of the CORDIC algorithm can be expressed as:

$$\delta \arctan\left[2^{-(n-1)}\right]_{\max}. \tag{A.1}$$

Consequently, the maximum approximation error $\delta_{\max}$ of the CORDIC algorithm can be regarded as a function of the iteration count n. It is evident that this function exhibits a monotonically decreasing trend within its domain and approaches 0 as $n \to +\infty$. The local curve of this function is shown in Fig. A1.

Since the computation is based on fixed-point arithmetic numerical iteration, during angle calculation using the CORDIC algorithm its accuracy directly relates to the data bit-width b in the iterative process. The quantisation error caused by finite precision in each iteration is termed the rounding error ϵ. Influenced by iteration, ϵ accumulates as follows:

$$\varepsilon = e(n) + \sum_{j=1}^{n-1} B(j)e(j), \tag{A.2}$$

where, $e(n)$ is the round-off error vector generated in the n iteration, $\sum_{j=1}^{n-1} B(j)e(j)$ is the cumulative rounding error vector from previous $n-1$ iterations, $B(j) = \prod_{i=j}^{n-1} \sqrt{1+2^{-2i}}$.

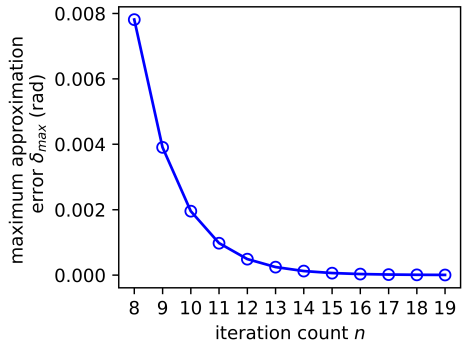

Fig. A1. Schematic diagram of the maximum approximation error.

For the error vector $e(n) = \begin{bmatrix} e_x(n) & e_y(n) \end{bmatrix}^T$:

$$\begin{cases} |e_x(n)| \le 2^{-(b-1)} \\ |e_y(n)| \le 2^{-(b-1)} \end{cases}. \tag{A.3}$$

Thus, the bound of $|e(n)|$ is:

$$|e(n)| \le \sqrt{e_x^2(n) + e_y^2(n)} \le 2^{0.5-b}. \tag{A.4}$$

The maximum rounding error $\varepsilon_{\max}$ is:

$$\varepsilon_{\max} = 2^{0.5-b} \left(1 + \sum_{j=1}^{n-1} \prod_{i=j}^{n-1} \sqrt{1 + 2^{-2i}} \right). \tag{A.5}$$

Consequently, the maximum rounding error $\varepsilon_{\max}$ is a function of iteration count n and data bit-width b. Its local curve is shown in Fig. A2.

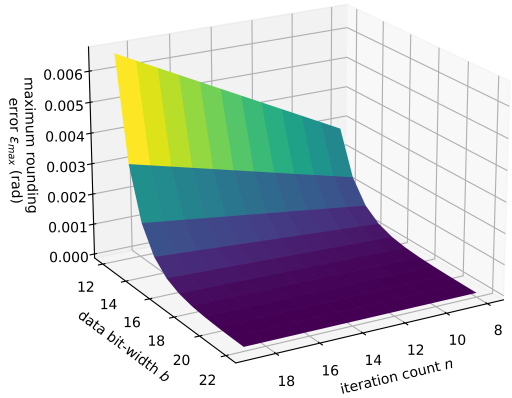

Fig. A2. Schematic diagram of the maximum rounding error.

Taking into consideration the maximum allowable error for the computation of the harmonic function, we set the iteration count $n = 16$ and the data bit-width $b = 18$.

References

[1] International Organization for Standardization. (2012). ISO 230-1:2012 – Test code for machine tools – Part 1: Geometric accuracy of machines operating under no-load or quasi-static conditions. ISO.

[2] Zou, W., Huang, Y., Lin, H., & Xue, Z. (2024). New application and research of ring laser gyroscope in the field of angle Metrology. *IEEE Transactions on Instrumentation and Measurement*, *73*, 1–12. https://doi.org/10.1109/tim.2024.3449940

[3] Lu, X., Graetz, R., Amin-Shahidi, D., & Smeds, K. (2010). On-axis self-calibration of angle encoders. *CIRP Annals*, *59*(1), 529–534. https://doi.org/10.1016/j.cirp.2010.03.127

[4] Lu, X., & Trumper, D. (2007). Self-Calibration of on-axis rotary encoders. *CIRP Annals*, *56*(1), 499–504. https://doi.org/10.1016/j.cirp.2007.05.119

[5] Watanabe, T., Fujimoto, H., Nakayama, K., Masuda, T., & Kajitani, M. (2001). Automatic high-precision calibration system for angle encoder. *Proceedings of SPIE, the International Society for Optical Engineering, vol. 4401*, 267. https://doi.org/10.1117/12.445630

[6] Watanabe, T., Samit, W., Vatcharanukul, K., Tonmueanwai, A., & Drijarkara, A. P. (2014). High resolution SelfA rotary table by the interpolation signal calibration. *Key Engineering Materials*, *625*, 53–59. https://doi.org/10.4028/www.scientific.net/kem.625.53

[7] Ishii, N., Taniguchi, K., Yamazaki, K., & Aoyama, H. (2018). Development of super-accurate angular encoder system with multi-detecting heads using VEDA method. *Journal of Advanced Mechanical Design Systems and Manufacturing*, *12*(5), JAMDSM0106. https://doi.org/10.1299/jamdsm.2018jamdsm0106

[8] Geckeler, R. D., Fricke, A., & Elster, C. (2006). Calibration of angle encoders using transfer functions. *Measurement Science and Technology*, *17*(10), 2811–2818. https://doi.org/10.1088/0957-0233/17/10/036

[9] Geckeler, R. D., Link, A., Krause, M., & Elster, C. (2014). Capabilities and limitations of the self-calibration of angle encoders. *Measurement Science and Technology*, *25*(5), 055003. https://doi.org/10.1088/0957-0233/25/5/055003

[10] Hong-Sheng, W., Qi-Feng, Z., Dong, Q., & Bang-Hui, G. (2011). Filtering method of improving quality of grating Moiré fringe. *Optics and Precision Engineering*, *19*(8), 1944–1949. https://doi.org/10.3788/ope.20111908.1944

[11] Yang, R., Tan, K. K., Tay, A., Huang, S., Sun, J., Fuh, J., Wong, Y. S., Teo, C. S., & Wang, Z. (2016). An RBF neural network approach to geometric error compensation with displacement measurements only. *Neural Computing and Applications*, *28*(6), 1235–1248. https://doi.org/10.1007/s00521-016-2486-2

[12] Park, J. W., Nguyen, H. X., Tran, T. N., & Jeon, J. W. (2021). A linear compensation method for improving the accuracy of an absolute multipolar magnetic encoder. *IEEE Access*, *9*, 19127–19138. https://doi.org/10.1109/access.2021.3054362

[13] Zhao, C., Wan, Q., & Liang, L. (2024a). Automatic compensation system for eccentricity error of absolute optical encoder. *Review of Scientific Instruments*, *95*(7). https://doi.org/10.1063/5.0211297

[14] Zhao, G., Ban, Y., Zhang, Z., Wang, X., Chen, B., Shi, Y., Jiang, W., & Liu, H. (2024). Error compensation strategy with high installation tolerance for angle encoders. *Precision Engineering*, *91*, 568–576. https://doi.org/10.1016/j.precisioneng.2024.10.017

[15] Zhou, Y., Zhu, W., Shu, Y., Huang, Y., Zou, W., & Xue, Z. (2022). Analysis and application of real-time compensation of positioning precision of the turntable with a harmonic function. *Metrology and Measurement Systems*, 553–571. https://doi.org/10.24425/mms.2022.142269

[16] Gurauskis, D., Kilikevičius, A., Borodinas, S., & Kasparaitis, A. (2019). Analysis of geometric and thermal errors of linear encoder for real-time compensation. *Sensors and Actuators A: Physical*, *296*, 145–154. https://doi.org/10.1016/j.sna.2019.06.055

[17] Zhao, C., Wan, Q., & Liang, L. (2024b). Automatic compensation system for small absolute optical encoders. *IEEE Sensors Journal*, *24*(19), 29778–29785. https://doi.org/10.1109/jsen.2024.3442916

[18] Takahashi, N., Watanabe, T., & Tobita, K. (2025). SelfA-inclinometer: A novel device for evaluating the accuracy of tilting rotary tables in five-axis machine tools. *Precision Engineering*, *95*, 38–51. https://doi.org/10.1016/j.precisioneng.2025.04.009

[19] Huang, Y., Xue, Z., Qiao, D., Wang, Y., Yue, C., Liu, G., & Wang, Z. (2016). Study on the metrological performance of self-calibration angle encoder. *Proceedings of SPIE, the International Society for Optical Engineering*, vol. *9684*. https://doi.org/10.1117/12.2246004

[20] Huang, Y., Xue, Z., Huang, M., & Qiao, D. (2018). The NIM continuous full circle angle standard. *Measurement Science and Technology*, *29*(7), 074013. https://doi.org/10.1088/1361-6501/aac6a6

[21] Kim, J., Kim, J. W., Kang, C., Jin, J., & Eom, T. B. (2013). Calibration of angle artifacts and instruments using a high precision angle generator. *International Journal of Precision Engineering and Manufacturing*, *14*(3), 367–371. https://doi.org/10.1007/s12541-013-0051-9

[22] Wang, Y., Xue, Z., Huang, Y., & Wang, X. (2016). Study on self-calibration angle encoder using simulation method. *Proceedings of SPIE, the International Society for Optical Engineering*, *9903*. https://doi.org/10.1117/12.2217638

[23] Zhao, J., Ou, W., Cai, N., Wu, Z., & Wang, H. (2024). Measurement Error Analysis and Compensation for Optical Encoders: A review. *IEEE Transactions on Instrumentation and Measurement*, *73*, 1–30. https://doi.org/10.1109/tim.2024.3417589

[24] Gao, W., Ibaraki, S., Donmez, M. A., Kono, D., Mayer, J., Chen, Y., Szipka, K., Archenti, A., Linares, J., & Suzuki, N. (2023). Machine tool calibration: Measurement, modeling, and compensation of machine tool errors. *International Journal of Machine Tools and Manufacture*, *187*, 104017. https://doi.org/10.1016/j.ijmachtools.2023.104017

[25] Shao, K., Zhu, W., Huang, Y., Xue, Z., Zhu, J., Kong, M., Zou, W., & Yin, Z. (2025). A study of the crucial parameters of Fourier method for improving the precision of rotary table. *Measurement*, *256*, 118390. https://doi.org/10.1016/j.measurement.2025.118390

[26] Andraka, R. (1998). A survey of CORDIC algorithms for FPGA based computers. In *Proceedings of the 1998 ACM/SIGDA Sixth International Symposium on Field Programmable Gate Arrays* (pp. 191–200). Association for Computing Machinery. https://doi.org/10.1145/275107.275139

[27] *AMD Zynq^{TM} 7000 SoCs*. (n.d.). AMD. Retrieved 7 July 2025 from https://www.amd.com/en/products/adaptive-socs-and-fpgas/soc/zynq-7000.html

[28] Li, G., He, Y., Gong, Z., Zhao, X., & Zhang, L. (2025). Deformation characteristics and angular error compensation of taper-mounted circular grating optical encoders. *Measurement*, *253*, 117694. https://doi.org/10.1016/j.measurement.2025.117694

Kairu Shao received his B.Sc. degree from China Jiliang University in 2023. He is currently pursuing his M.Sc. degree at China Jiliang University. His research interest is angle measurement.

Zi Xue received her Ph.D. degree from Harbin Technical University in 2006. She joined the Division of Metrology in Length and Precision Engineering of the National Institute of Metrology in 1991. Her main research interest is geometric measurement.

Weibin Zhu (corresponding author) received his Ph.D. degree in control theory and engineering from Zhejiang University in 2014. He is currently a professor at China Jiliang University. His current interests include grating signal processing and precision angle measurement.

Jin Zhu received his M. Sc. degree from China Jiliang University in 2022 and is currently working at Zhejiang Institute of Quality Sciences. His main research interest is geometric measurement.

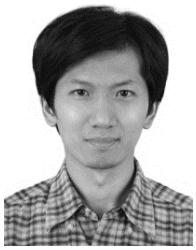

Yao Huang received his Ph.D. degree from Zhejiang University in 2025. He worked at the Geometric Lab of the Beijing Institute of Metrology from 2007 to 2013 and joined the Division of Metrology in Length and Precision Engineering of the National Institute of Metrology in 2013. His main research interest is angle measurement.